SOHO INTO BOGART:

Rescaling a Successful Mission to Support Living With a Star

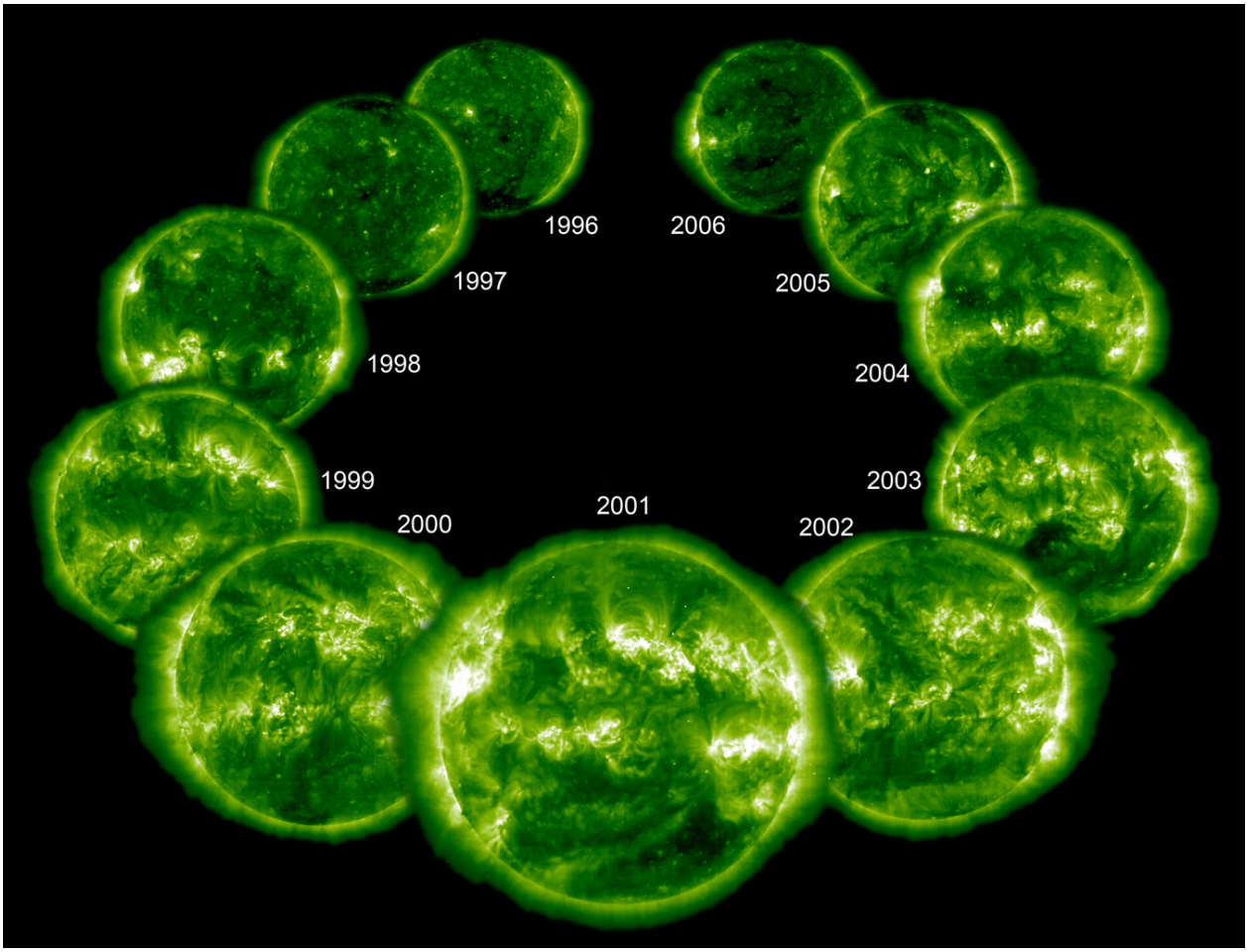

A PROPOSAL TO THE SENIOR REVIEW OF HELIOPHYSICS OPERATING MISSIONS, 2008 FEBRUARY.

Table of Contents

Solar and Heliospheric Observatory (SOHO)

Presenters: J.B. Gurman, US Project Scientist for *SOHO*

I. Executive Summary

This is the fifth Senior Review proposal from *SOHO*, but we are not requesting an extension of the mission that has led to so many exciting discoveries and so much deeper understanding of the Sun and heliosphere, from the deep solar interior to the interstellar medium. Instead, we propose here a dramatically descoped mission that nevertheless fulfills the requirement of the Living With a Star program's Solar Dynamics Observatory (SDO) mission for a white-light coronagraph to provide a Sun-Earth line view of both the evolution of and transient events in the solar corona.

In the next section of this proposal (***Section II***), we summarize the widespread use and easy accessibility of *SOHO* data.

In ***Section III***, we discuss just a few of the many insights into the physics of the Sun, heliosphere, and beyond from the analysis of *SOHO* observations since late 2005, when our last senior review proposal was submitted. All of these highlights are directly relevant to the basic science question posed in NASA's Science Mission Directorate *Science Plan, 2007 - 2016: "How and why does the Sun vary?"* More specifically, they address many critical facets of the research objective, "*Understand the fundamental physical processes of the space environment from the Sun to Earth, to other planets, and beyond to the interstellar medium*." In that section, you will find, among many other highlights, descriptions of specific enhancements in methodologies to be employed in interpreting SDO HMI observations, and dramatic improvements in forecasting solar flares and SEP events.

SOHO has done its part by providing a nearly continuous record of solar and heliospheric phenomena for one activity cycle (that is, half the magnetic cycle); it is now the turn of newer missions, such as *Hinode*, STEREO, and SDO – the lineal descendent of *SOHO*. A subset of *SOHO*'s services are still needed to fill a critical lacuna in SDO's instrument complement, however, and ***Section IV*** describes how, like Humphrey Bogart's regular reduction of cigarettes to the last nubbin, we propose to use *SOHO* capabilities throughout the nominal SDO mission lifetime in a "Bogart" mission that will depend on operating *SOHO*, the truly great observatory-class spacecraft in the HGO fleet, on a Small Explorer (SMEX) budget (***Section V***). Although only the LASCO coronagraphs can meet the SDO coronagraphy requirement, for virtually no operational or resource overhead, *SOHO* will continue to be able to provide total solar irradiance, integrated EUV solar output, low-frequency global solar oscillation, energetic particle, and solar wind *in situ* plasma measurements.

Section VI provides a description of the necessarily circumscribed education and public outreach activities we hope to continue into the Bogart mission.

The following individuals were among those involved in the writing of this proposal on behalf of the *SOHO* Science Working Team: J.B. Gurman (GSFC), J. Kohl, S. Cranmer, L. Gardner, J. Raymond, L. Strachan (SAO), F. Ipavich (U. Md.), P. Scherrer and A. Kosovichev (Stanford U.), R. Howard (NRL); B. Fleck (ESA), E. Quémerais (SdA), W. Curdt (MPS), C. Fröhlich (PMOD/WRC), A. Fludra (RAL), B. Klecker (MPE), Reinhold Müller-Mellin (U. Kiel), and E. Valtonen (U. Turku). We would also like to thank the S&H Guest Investigators who provided material for this proposal.

II. Data Accessibility

Ubiquity. *SOHO* enjoys a remarkable "market share" in the worldwide solar physics community: over 3,000 papers in refereed journals since launch (not counting refereed conference proceedings, which generally duplicate journal articles), representing the work of over 3,000 individual scientists. Even accounting for the number of "heliospheric" papers and authors in those numbers, it is not too much of an exaggeration to say that virtually every living solar physicist has had access to *SOHO* data.

Accessibility. We can assert that with confidence because all the *SOHO* experiments make all their data available, online, on the Web, through the *SOHO* archive, at PI sites, and via the Virtual Solar Observatory (VSO). A typical PI site, the EIT Web catalog, has served over 1.2 Tbyte of data in response to over 1,000 requests since early 2006 — and the EIT database was only 700 Gbyte at the end of 2007. The larger MDI database, which includes several levels of computationally expensive, higher-level data products, has served over 17 Tbyte in response to over 10,000 online data requests in the last two years. (This total does not include an equal volume of larger data exports shipped to Co-Investigator and Guest Investigator sites on tape.) In addition to professional access, amateurs routinely download LASCO FITS files and GIF images to search for new comets. As a result, nearly half of all comets for which orbital elements have been determined (since 1761) were discovered by *SOHO*, over two thirds of those by amateurs accessing LASCO data via the Web. 115 of the 177 comet discoveries in the last year confirmed by the IAU were made with *SOHO* observations. One, comet P/2007 R5, was determined by a radio astronomy graduate student who works on comets in his spare time to be the first periodic comet discovered from *SOHO* observations.

Research access. All *SOHO* instruments' scientific data are accessible through a single interface, http://soho.nascom.nasa.gov/data/archive/ . This searches both the general *SOHO* archive at the Solar Data Analysis Center (SDAC) at Goddard, and the MDI high-rate helioseismology archive at Stanford. (MDI full-disk magnetograms obtained every 96 minutes are part of the general archive, because of their usefulness for solar activity-related research.) In both archives, the holdings are identical to those used by the PI teams, and are current (*i.e.* to within a month or two before present, to allow time for "Level-Zero" data delivery.) Partial mirrors of the *SOHO* archive are maintained at the Institut d'Astrophysique Spatiale (France) and the University of Torino (Italy) for faster access by European researchers. *SOHO* data at both the SDAC and the Stanford Helioseismology Archive were among the first data whose metadata, including browse images for EIT and MDI, became searchable *via* the VSO. The VSO is designed to deliver data *via* the original servers, so the download traffic still occurs at those sites.

Publications. The *SOHO* publications database can be accessed at:
http://sohodata.nascom.nasa.gov/cgi-bin/bib_ui .

III. Scientific Insights from SOHO, 2006 - 2007

The following, brief descriptions of scientific insights gained from *SOHO* have been gleaned from papers published in, or recently submitted to, refereed journals since the 2006 Senior Review; a few results from recent conference proceedings are also included. Scientific insights from earlier phases of the mission were covered in the proposals to the 1997, 2001, and 2003, and 2006 Senior Reviews.

From the Sun...

The Solar Interior and Total Irradiance

Total Solar Irradiance

The total solar irradiance (TSI) record from the VIRGO radiometers now extends over 12 years. Significant differences in their designs have made it possible to determine and eliminate instrumental aging from the record of VIRGO, and the methods could also be applied to the earlier TSI records used for the composite (Fröhlich 2006). Even though solar minimum had not occurred by the end of 2007, TSI dropped below the solar minimum value of 1996. Indices such as the MgII index, the 10.7 cm flux or the sunspot number do not show a decrease similar to TSI, but the flux in the open magnetic field (from OMNI2) does. This field is also responsible for the modulation of the galactic cosmic rays and determines the production of the cosmogenic isotopes. This result will improve our understanding of the connection between TSI and cosmic rays, which up to now had to be based on correlations only.

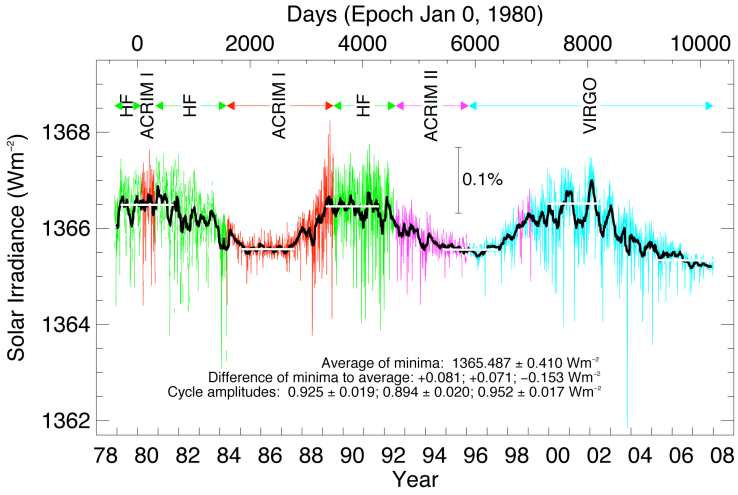

Figure 1. The composite total solar irradiance (TSI) for three solar cycles, combining data from multiple spacecraft instruments; different colors indicate different data sources.

The Solar Interior

Statistical evidence for g-modes. García *et al.*(2007) concluded, on the basis of an analysis of ten years of GOLF observations, that the power in a range of periods around 24 minutes was consistent with a model of *g*-modes (buoyancy modes) with radial orders of $n = -4$ to $n = -26$, at the $> 3\sigma$ level. This degree of significance, however, is far from conclusive and there is a divergence of opinion in the *g*-mode community regarding the significance of this result as a detection of the long-sought modes believed to exist deep in the solar interior.

Meridional flows and magnetic flux transport. Švanda et al (2007) used magnetic synoptic maps to determine the speed of magnetic flux transport on the solar surface towards the poles throughout cycle 23. The manifestation of flux transport is clearly visible as elongated structures extending from the active latitudes to the polar regions (Figure 2). Svanda *et al.* (2007) interpreted the slopes of these structures as the meridional magnetic flux transport speed.

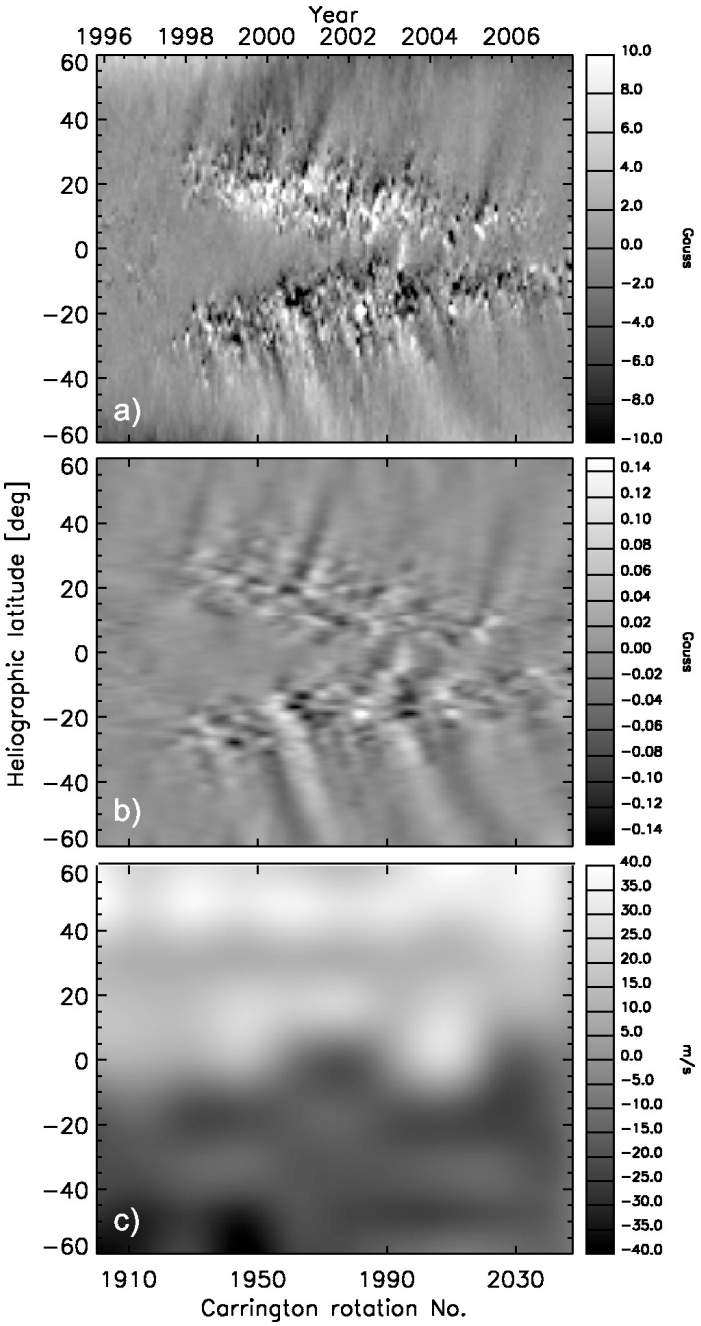

Figure 2. a) The magnetic synoptic diagram for cycle 23. b) The filtered magnetic synoptic diagram showing enhancements of the flux transport elongated structures. c) The measured meridional flux transportation speed (in the South–North direction) for Carrington rotations 1900-2048.

Comparison with the time-distance helioseismology measurements of the mean speed of the meridional circulation at depths of 3.5 - 12 Mm from MDI measurements shows a generally good agreement with the values derived from magnetic flux transport, but the speed of the magnetic

transport and meridional flow are significantly different in areas occupied by the magnetic field. The local circulation flows around active regions (Fig. 3), especially the strong equatorward flows on the equatorial side of the active regions affect the mean velocity profile derived by helioseismology, but they do not influence the magnetic flux transport. The formation of an apparent counter-cell appears to be a common property of all large active regions at depths of 3 – 12 Mm.

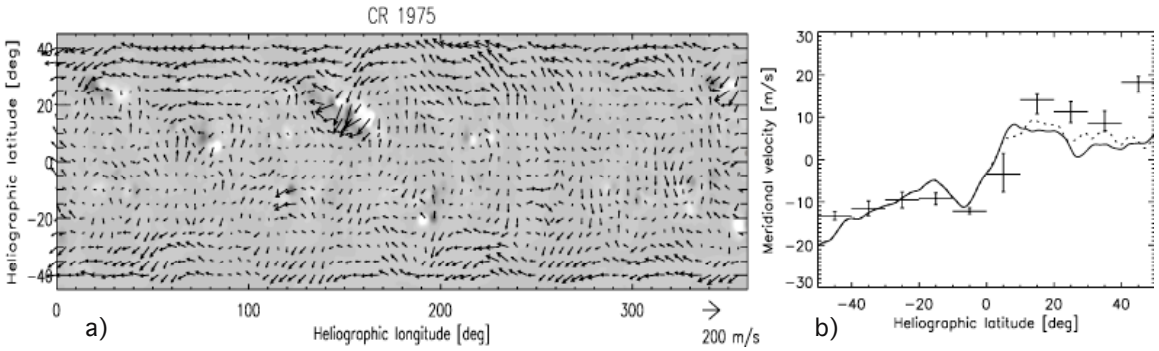

Figure 3. (a) A large-scale flow map at depth 3 – 4.5 Mm for Carrington rotation 1975 (2001 April), with the corresponding MDI magnetogram-derived synoptic map as the grey-scale background. Large-scale flows towards equator in the magnetic regions are visible around the large active region. (b) The longitudinally averaged meridional circulation profile for the same Carrington rotation. The southern hemisphere shows almost no magnetic activity, so the meridional circulation profile obtained by averaging the time-distance flow map (solid line) almost fits the magnetic flux transport profile (points with error-bars) there, while in the northern hemisphere there are significant differences.

The results show that the mean longitudinally averaged meridional flow measurements derived from time-distance helioseismology alone cannot be used directly in solar dynamo models for describing the magnetic flux transport, and that it is necessary to take into account the longitudinal structure of these flows. This is a major lesson for the interpretation of SDO HMI observations.

Apparent solar cycle variation in solar oblateness. The Sun's shape is sensitive to the influence of gravity, rotation, and local turbulence and magnetic fields in its outer atmosphere. A careful measurement of this shape has long been sought to better understand the solar structure and its change over the 11 year solar activity cycle. Numerous, disparate measurements of the solar oblateness or the fractional difference between equatorial and polar radii have been difficult to interpret, in part because this quantity is much smaller than terrestrial atmospheric seeing and most instrumental noise sources. In 1997, MDI obtained a precise measurement of the oblateness from above the atmosphere by utilizing a spacecraft roll procedure to remove instrumental influences on measurements of the diameter. In 2001, during solar maximum, this technique was repeated, and Emilio *et al.* (2007) derive a significantly different oblateness from these data than that from the 1997 measurements (Fig. 4).

The changes they found are smaller than the apparent discrepancies among earlier ground-based observations, but significantly larger than MDI's astrometric measurement uncertainty. The shape change appears to be anticorrelated with the observed helioseismic variability. This fact and the MDI measurements suggest that the outer solar atmosphere expands nonhomologously during the

cycle. It is possible that solar cycle changes in the turbulent pressure in the outer atmosphere can account for both the optical limb change and the helioseismic acoustic global solar shape change.

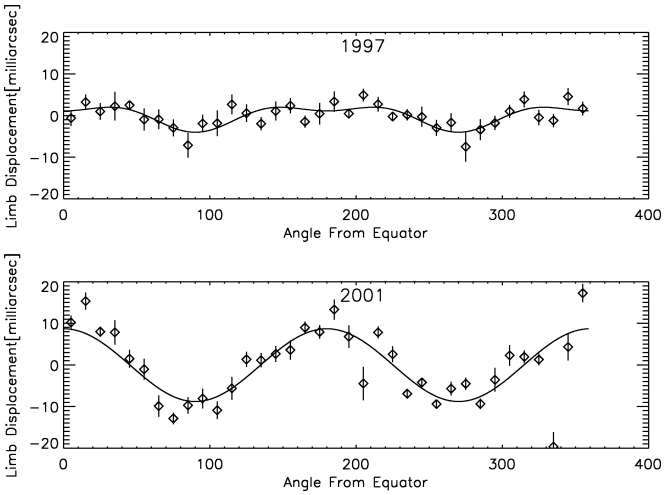

Figure 4. Limb shape from 1997 (solar minimum) and 2001 (solar maximum) is plotted here. The equator corresponds to position angles 0 and 180. Data have been averaged into 10° wide bins, and the best fit (oblateness) and (hexadecapole) Legendre polynomial have been plotted. The shape distortion after correcting for bright contamination is nearly a pure oblateness term in 2001, while 1997 has a significant hexadecapolar shape contribution.

The Solar Atmosphere

The abundance of neon. As noted in our 2006 proposal, work by Asplund *et al.* (2004) lowered the estimate of the solar photospheric abundance of oxygen by nearly a factor of 1.5 below previous estimates. That work also thereby lowered estimates of the solar neon abundance by a similar amount, since the neon abundance is usually found by reference to the neon-to-oxygen abundance ratio. The lower abundances were questioned by the helioseismological community, as both sound speed values near the tachocline and neutrino production rates from "standard" models were found to diverge from results of global helioseismological inversions and neutrino measurements, respectively. A potential solution involved an increase in the photospheric neon abundance by a factor of 2.5 over Asplund *et al.*'s value; neon abundances are typically suspect because there are no solar photospheric neon lines. In work just too late to be included in our last proposal, Young (2005), however, used CDS measurements of the ratio of neon and oxygen abundances in the upper chromosphere and transition region (in which there is believed to be no fractional ionization relative to the photosphere) to conclude that Asplund *et al.*'s value, log A(Ne) = 7.84 ± 0.06 on a scale where log A(H) = 12, was in good agreement with the CDS measurements, which yielded log A(Ne) = 7.89 ± 0.16.

Magnetoacoustic waves in the transition region and corona. Using simultaneous CDS measurements of oscillations in lines formed at transition region and coronal temperatures, O'Shea *et al.* (2006) found evidence for outward-propagating waves above the solar poles. They interpreted phase differences between various pairs of lines as evidence for fast magnetoacoustic waves at coronal temperatures, and slow magnetoacoustic waves at lower temperatures, and statistically significant peaks in the phase difference spectra near 90° as evidence for the presence of a resonant cavity. O'Shea *et al.* (2007) extended this work to coronal holes observed on the solar disk, where they found propagating, slow magnetoacoustic wave power in regions of enhanced EUV emission within the holes.

Downward propagating waves. Gömöry *et al.* (2006) used CDS measurements of oscillations at transition region and chromospheric heights to argue that the observed phase delay matched the prediction of Hansteen's (1993) model of downward-propagating compressive waves excited by nanoflares in the corona. In the light of the recent detection of a considerable Alfvén wave flux in the upper chromosphere (De Pontieu *et al.* 2007), however, it is not clear whether a nanoflare model of coronal heating is still viable.

Bright points and reconnection. Using measurements obtained by EIT over some three days of the intensities of bright points in He II 304 Å, McIntosh (2007) found rings in the skew and kurtosis distributions around the bright points that are consistent with continuous, magnetoconvectively driven reconnection to the supergranular magnetic field.

Ubiquitous downflows. Both solar and cool stellar transition regions show systematic downflows in emission lines formed at transition region temperatures. Doschek (2006), using SUMER measurements of lines formed at 0.10 - 0.14 MK and one at 0.8 MK, found little correlation between the Doppler shifts in the cool lines and the hotter one, and so concluded that the lower-temperature transition region lines are formed in cool loops containing no coronal material, and that the loops must be continuously heated to produce downflowing condensations at the observed temperatures.

Coronal loops: isothermal or multithermal? One of the outstanding questions in the physics of the outer solar atmosphere is whether the plasma in fine loops observed in the EUV is nearly isothermal, or thermally stratified. The vigorous debate continued over the last two years, with Schmelz and Martens (2006) showing conclusively that the loops they studied with CDS could not be isothermal, while Cirtain *et al.*(2007), using both TRACE imagery and CDS spectra, found that for sufficiently fine (< 2 arc sec wide) loops, there were times ("often but not always") when a single temperature matched their differential emission measure determinations of plasma temperatures in the loops. The solution to this persistent issue may have to wait for high temporal and spatial resolution imaging in conjunction with high spatial resolution spectroscopy.

Polar coronal plumes. EUV- and soft X-ray-bright plumes emerging from polar coronal holes have been of interest for nearly two decades: do they contribute to high-speed solar wind streams? Are they cooler material unconnected with the plasma sampled at high latitude by *Ulysses*? Curdt *et al.* (2008) carried out a new series of polar plume observations with SUMER in conjunction with early *Hinode* and STEREO measurements. They found that the spatial variation in the ratio of emission in a Ne (high-FIP) line to that in a line of Mg (low-FIP) defined the pattern of plumes even more clearly than did a density-sensitive line ratio diagnostic.

Pseudostreamers: a source for high-speed wind? Wang *et al.* (2007) have distinguished "pseudostreamers" in LASCO images from true helmet streamers that overlie polarity reversal lines. The pseudostreamers represent coronal density enhancements overlying pairs of loop arcades and rooted in regions of the same magnetic polarity. Figure 5 shows the magnetic field of a pseudostreamer observed by LASCO. From earth or L1, the geometry is difficult to distinguish from a normal helmet streamer, but rotating the view angle by 90^{o} shows that the field is in fact open to the solar wind. The authors speculate that two types of interchange reconnection are possible in such an X-type neutral point geomtery: closed loops may undergo 3D reconnection with an open

field line rooted next to it., and closed loops may also reconnect with an open field line rooted in a more distant coronal hole, resulting in the transfer of open and closed flux in opposite directions across the X-point. The authors therefore expect pseudostreamers to be sources of high-speed wind, and may provide the best means to observe the fast wind near its origin.

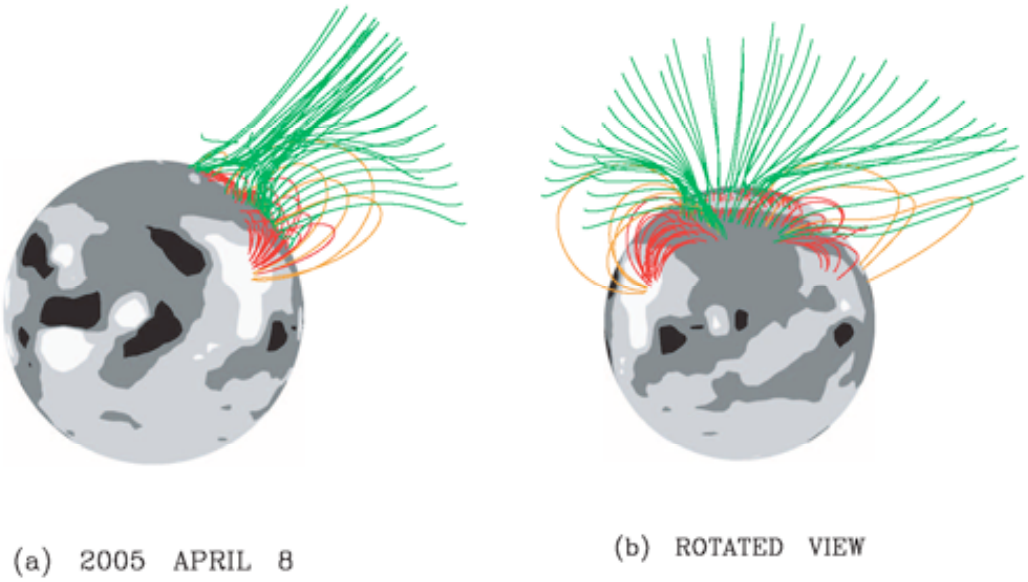

Figure 5. PFSS magnetic field extrapolations (from groundbased magnetography) for a pseudostreamer observed in 2005. Open field lines are in green*, closed field lines in* orange *if they extend beyond 1.5 solar radii and* red *if they do not extend so far.*

Coronal Mass Ejections and Flares

Predicting solar flares from magnetic topology. Georgoulis and Rust (2007) defined an "effective connected magnetic field," B_{eff}, from a matrix of strongly connected magnetic flux concentrations in active regions from ten years (1996 - 2005) of MDI magnetograms. Identifying 298 active regions (93 producing M- and/or X-class flares, 205 without large flares) in their data, they found that B_{eff} is a robust criterion for identifying regions likely to have large flares: a well-defined, conditional probability for a large flare within 12 hours depends only on B_{eff}, and the probability exceeds 0.95 for M and X flares when $B_{eff} > 1600$ and 2100 gauss, respectively. No M flares occur within 12 hours when $B_{eff} < 200$ gauss, and no X flares when $B_{eff} < 750$ gauss. Schrijver (2007), also using MDI magnetograms to study 289 M- and X-class flares, found that the total unsigned flux within 15 Mm of high field gradient polarity reversal lines – a telltale of magnetic fibrils carrying strong electric currents – could similarly be used to predict large flares with similar accuracy.

The nature of "EIT" waves. Wills-Davey *et al.* (2007) found that coronal waves observed by EIT in conjunction with CMEs are poorly explained as fast-mode MHD waves; instead, they propose a

soliton solution that is in better agreement with the speeds and single-pulse nature of the "EIT waves."

Modeling CMEs as Flux Ropes. The identification of a CME as a magnetic-flux rope (Chen *et al.* 1997) was tested by Thernisien *et al.* (2006), who applied a geometric model of flux-rope structure to 34 of the CME events analyzed by Cremades and Bothmer (2004). Using observed properties of the source regions to specify parameters defining the orientation and size of the model flux rope, and then fitting the remaining model parameters by matching the observed intensities of the CME front with the intensities computed from the Thomson scattering from the electron density distribution determined from LASCO measurements, they obtain geometrically convincing results (Figure 6). The model is intended to represent only the flux rope, not the internal structure associated with *e.g.* trailing prominence material. Detailed comparisons of radial profiles with the observed CME fronts is excellent, except for an indication of material ahead of the leading edge, with ~ 0.1–0.2 of the peak density. That could be an indication of a coronal wave ahead of the CME, but needs further analysis. Another geometric model comparing flux ropes and observed CMEs was tested by Krall and St. Cyr (2006), with similar results.

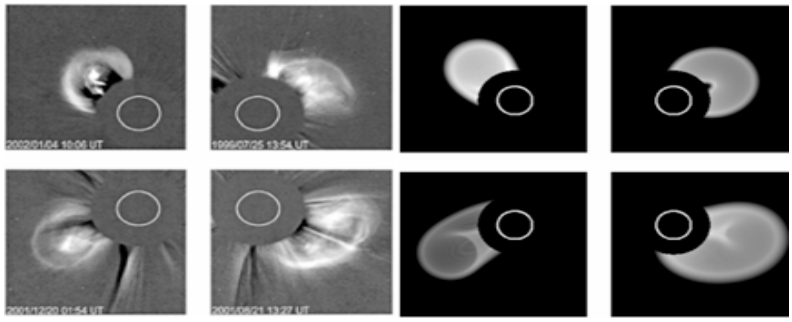

Figure 6. Left four panels: *LASCO images of four different CMEs analyzed by Crmades and Bothmer (2004);* right four panels: *flux-rope model calculations for the same CMEs by Thernesien et al. (2006).*

3-D diagnostics. Lee *et al.* (2006) used UVCS observations to analyze a fast CME associated with an X flare to determine the three-dimensional distribution of velocities, densities, temperatures, and heating rates. They found that hot plasma observed in the Fe XVIII forbidden line (formed at temperatures of ~ 5 MK) was located within a bubble of cooler material emitting in O VI, and within a much more concentrated volume. Lee (2007) extended this work to determine the heating rates for 14 features in a CME and found that neither thermal conduction nor wave heating at quiet-Sun rates could account for the heating. Bemporad *et al.* (2007), mapping out the shape of the "leading edge" of a slow CME not associated with a flare or filament eruption, showed that 2/3 of the CME mass originated *above* 1.6 solar radii. They also found that the CME plasma was hottest in the bright core, consistent with the predictions of Kumar and Rust (1996) for the conservation of magnetic helicity in an expanding flux rope.

CME shocks and SEP seed particles. UVCS spectra provide an unambiguous means of observing the shocks associated with some CMEs. The halo CME study of Ciaravella et al. (2006) revealed 7

new shock wave detections out of 14 observations of CME fronts. Pagano et al. (2007) and Pagano (2008) are extending MHD models of CME shocks to predict line intensities, widths, and Doppler shifts for direct comparison to UVCS observations that will allow a more accurate determination of quantities such as the shock compression ratio and differences between electron and ion temperatures. By measuring the detailed shape of the H I Lyα emission line, Kohl et al. (2006b, 2007) demonstrated that UVCS has the sensitivity to distinguish between a Maxwellian coronal velocity distribution and a suprathermal "kappa" exponent of 4 or smaller. This value corresponds to the level of "seed particles" needed to exist in the corona to produce solar energetic particles (SEPs).

Solar magnetic field topology mapped onto an ICME. Attrill *et al.*(2006) argue that the canonical CME/coronal wave event of 1997 May 12 can be interpreted as two separate eruptions of mass and magnetic flux, with only the more southern of the two dimming regions observed with EIT responsible for the ICME observed by the WIND spacecraft. Their estimates of the magnetic flux erupting from the southern dimming region, based on a variety of field topology models, agree to within an order of magnitude with values derived from WIND *in situ* measurements.

CMEs and SEPs. Kahler and Vourlidas (2005) analyzed CMEs associated with SEP events to determine what CME observables could be used to predict SEP events at 1 AU, and found that SEP-rich CMEs are brighter and more likely to be streamer-blowout events, and more likely to follow colocated CMEs within 12 - 24 hours, than their SEP-poor counterparts. The enhanced brightness, and hence mass, of the SEP-rich events appears to be the most dominant characteristic, so that either exceptionally large or dense events are necessary for significant SEP fluences.

The interpretation of O VI line profiles in coronal holes. The interpretation of O VI observations in coronal holes. Raouafi et al. (2007) claimed that the broad profiles of O VI lines measured with UVCS in polar coronal holes (PCHs) could be explained without resort to a temperature anisotropy by the superposition of the velocity distribution in polar plumes at heliographic latitudes of 70^{o} - 80^{o}. Cranmer et al. (2008), however, employed a new analysis method to demonstrate that the UVCS measurements of O VI profiles and intensity ratios in PCHs are more consistent, at every height above 2.1 solar radii, with an anisotropic ($T_{perp} > T_{parallel}$) O VI ion temperature distribution than with an isotropic one. Both analyses show that oxygen ions are preferentially heated and accelerated with respect to hydrogen..

The Solar Wind

Solar wind acceleration. The high ion kinetic temperature interpretation of UVCS O VI line profiles has given rise to a resurgence of interest in collisionless wave-particle resonances (specifically the ion cyclotron resonance) as potentially important mechanisms for preferentially heating ions in the accelerating solar wind. Recent theoretical work has explored the kinetic microphysics that must be occurring in the extended corona in order to give rise to the observed preferential heating. For example, MHD turbulence may give rise to ion cyclotron waves via either shear instabilities (Markovskii et al. 2006) or via mode-coupling between Alfvén and fast-mode waves (Chandran 2005). Also, Hollweg (2006) found that the radial dependence of the O^{5+} temperatures measured by UVCS was more easily explainable with a combination of outward and inward propagating Alfvén waves than with just outward waves. This suggests some kind of wave reflection as a key process in coronal holes. Cranmer et al. (2007) found that turbulence enabled by such wave reflection can

produce a realistic range of slow and fast solar wind conditions by varying only the geometry of the coronal magnetic field.

Solar cycle dependence of the He^{++}/H^{+} ratio. Using WIND measurements, Aellig *et al.* (2001) found that the He^{++}/H^{+} ratio increased by roughly a factor of three between solar minimum in 1996 and 2000, shortly before solar maximum. Ipavich (private communication) has recently compared alpha particle data from ACE/SWICS and proton data from the CELIAS MTOF PM to find that the variation continues throughout Cycle 23 (Figure 7).

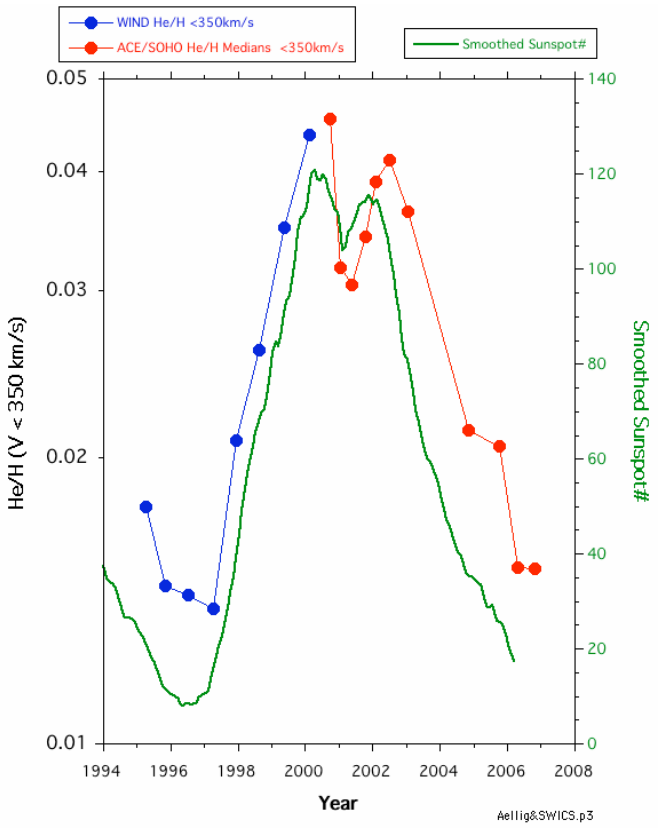

Aellig *et al.* (2001) made the reasonable suggestion that the reduced He^{++}/H^{+} at solar minimum was due to inefficient Coulomb drag, a strong function of the solar wind proton flux near the acceleration region (at a few solar radii). The model suggests that a stronger flux tube expansion at solar minimum produces a smaller proton flux, which in turn leads to a smaller He^{++}/H^{+} ratio. Since the Coulomb coupling is different for every ion in the solar wind, Ipavich plans to test the model further by examining the solar cycle dependence of oxygen and iron relative to hydrogen.

Figure 7. Time dependence of the slow solar wind He^{++}/H^{+} ratio.

Energetic particles, solar and cosmic ray

The interplanetary highway revisited. As noted in the last *SOHO* Senior Review proposal, ERNE was used to study the "Interplanetary highway" event of May 2 1998 (Torsti *et al.* 2004). This event was observed when SOHO spacecraft was inside a magnetic flux rope, and the very low scattering conditions inside the cloud enabled the energetic particles to reach the ERNE particle sensors almost unimpeded by the transport effects. By using the uniquely accurate angular resolution of the ERNE High Energy Detector (HED), Kocharov et al. (2007a) were able to study the evolution of the energetic particle transport throughout the event in detail. Using Monte Carlo simulations, they discovered that the spacecraft, while observing the event, traversed through flux tubes with extremely different energetic particle transport conditions (Figure 8), starting with up to 20 AU scattering mean free path during the first hours of the event, and decreasing, in several steps, to just 1.5 AU, which still is long compared to average interplanetary transport conditions. The accurate an

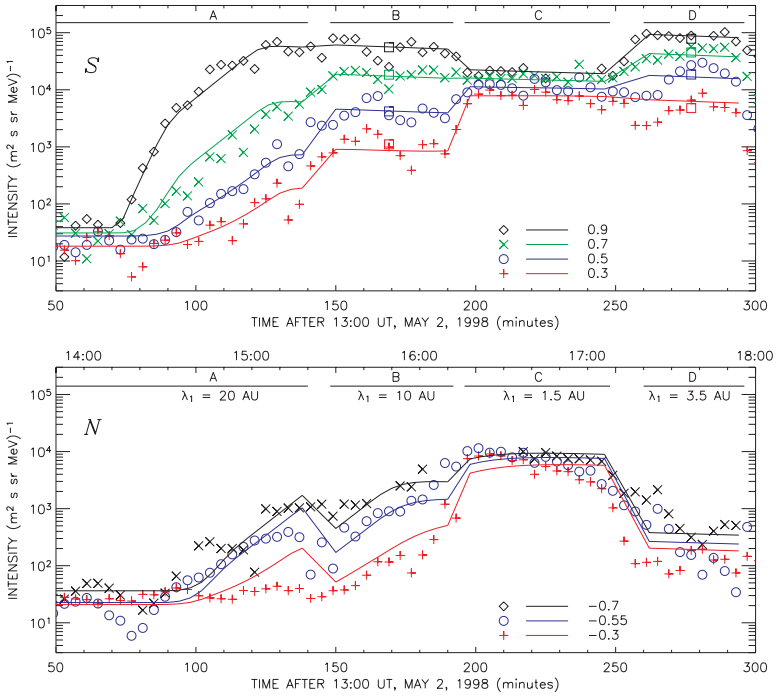

gular resolution proved to be critical in probing the magnetic cloud structure by energetic particle streams.

Figure 8. Intensity-time profiles of 17--22 MeV protons arriving at different angles with respect to the magnetic field (points)*, compared to simulations* (solid lines)*, from the southern directions (top) and from the northern directions (bottom). Pitch angle cosines (0.3, 0.5, 0.7, 0.9) are shown in the figure legends. The horizontal bars A, B, C and D depict different periods with different energetic particle mean free paths.*

The extremely low level of particle scattering is advantageous for the analysis of the temporal and spatial origin of the energetic particles, and the connection of the particle eruption to other solar plasma and electromagnetic observations. Kocharov et al. (2007b) concluded in their work that the observations clearly show a two-component injection process for the energetic particles. The first injection, up to tens of MeV in proton energies, was rapid and energy-dependent, and well-correlated with the beginning of a coronal wave observed by EIT start and a radio flash, suggestive of acceleration on open field lines. This was followed 15 minutes later by a more gradual injection, temporally associated with an EIT dimming, and occurring simultaneously at energies up to a few hundreds of MeV in ERNE and earth-based neutron monitor measurements. The nature and temporal associations of the second injection suggest that the acceleration of these particles took place on initially closed field lines, which then opened due to coronal restructuring of the magnetic fields, allowing the particles to escape to interplanetary space. The detailed analysis of this solar energetic particle event was made possible by the exceptionally good "seeing" conditions, with the high-energy particles inside an interplanetary magnetic cloud, which resulted in smaller than usual uncertainties in determining the timings of the solar particle release.

...to Earth...

Seasonal variations of electron upstream events. Energetic electrons with energies ≤ 0.220 MeV (e.g. Fan et al., 1964) and ions with energies <1 MeV (e.g. Asbridge et al., 1968) upstream of the Earth's bow shock, preferentially streaming from the magnetosphere/bow shock in the Sunward direction, have been observed for over forty years. Most of such upstream bursts were observed near the bow shock at ~25 R_e, but also far upstream from the bow shock at L1 (~240 R_e). The upstream ion bursts often associated with energetic (E > 30 keV) electrons were explained by both the leakage of magnetospheric particles accelerated within the magnetosphere, and acceleration by the

bow shock. Most previous observations were made close to the bow shock and/or during relatively short periods. Using COSTEP EPHIN electron observations at E >= 0.250 MeV, Klassen et al. (2006) were able to extend those observations to distances far from the bow shock – at L1 – during nearly all of solar cycle 23 (1996 - 2005). They demonstrated that some upstream electron events are observed up to relativistic energies above 0.7 MeV. Almost all bursts have a time duration < 10 min and show nearly square or triangular pulse-shaped time profiles, which differ strongly from solar electron events. They also found that the event occurrence frequency shows a distinct seasonal variation with maxima around equinoxes and minima near solstices. Combined with a close correspondence between the event occurrence frequency and maxima in solar wind speed (V_{SW}), geomagnetic activity index (A_p) and in the southward interplanetary magnetic field (IMF) component (B_Z), this indicates that the observed events can be explained in terms of leakage of magnetospheric particles during enhanced geoactivity rather than by acceleration at the Earth's bow shock.

Thermospheric modeling. A new model (Tobiska *et al.* 2007) of terrestrial thermospheric density as a function of solar input uses an index based on CELIAS SEM EUV flux measurements, as well as the familiar F10.7 and Mg II indices to predict the behavior of the thermosphere as well as reproduce its behavior over solar cycle 23. The model will enable near-realtime prediction of satellite drag in operational environments.

...and beyond...

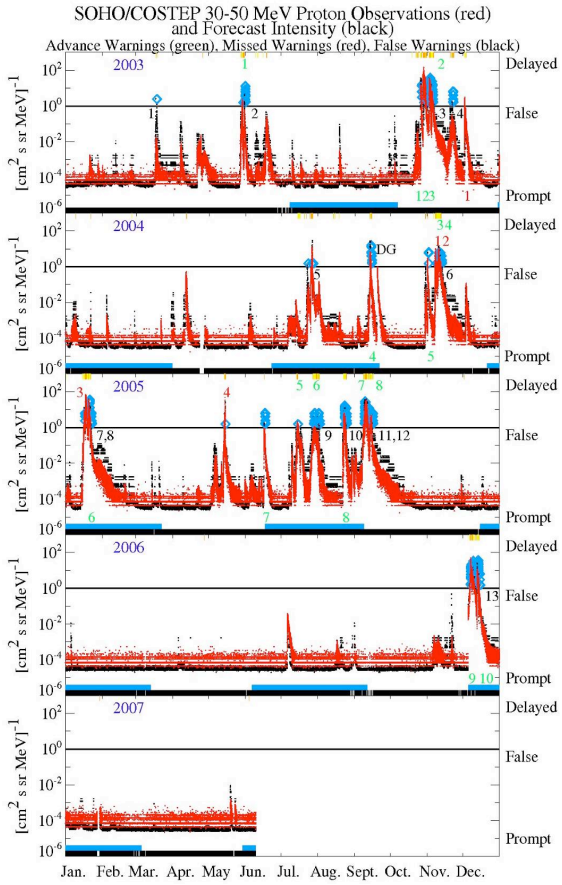

Figure 9. Application of the COSTEP forecasting method. In most of the events, the maximum intensity of the particle event is predicted half an hour before the proton onset.

Radiation hazard forecasting. Sudden increases in the fluence of >30 MeV protons in SEP events pose a hazard to human space activities and robotic space missions. Posner (2007) developed a method of forecasting the intensity of prompt solar energetic protons at hazardous energies using COSTEP measurements of the much faster relativistic (150 keV - 10 MeV) electrons in 1996 - 2002 as early warnings for the later (~ 0.5 hr) arriving protons (at 40 MeV) in prompt SEP events. The electrons act as test particles by probing the continuously changing heliospheric transport conditions in the same region of the heliosphere through which the slower-moving protons have to propagate. Heber et al. (2007) have recently extended the verification of the method with COSTEP data through 2007 (Figure 9) to confirm the high success rate, low miss rate, and low false positive rate of the method. ***We note that the SMD Science Plan, 2007 - 2016 calls for the ability to forecast hazards sometime after 2016 – but this SOHO***

COSTEP work promises to make accurate forecasting of hazardous SEP events a reality in solar cycle 24, which should help make it possible to "Safeguard the Journey of Exploration" during the next decade.

Anomalous cosmic rays. Energetic neutral atoms (ENAs) of hydrogen and helium are monitored by CELIAS HSTOF. Potential sources of ENAs in the heliosphere are CIRs, solar energetic particle events, pre-accelerated pickup ions as well as low-energy (up to a few hundred keV) anomalous cosmic ray (ACR) ions in the outer heliosphere, close to and beyond the solar wind termination shock. ENAs, neutralized via charge transfer reactions, can penetrate into the inner solar system, unaffected by the interplanetary magnetic field. The observed ENA fluxes from 1996 onward set limits on potential theories of the dominant sources of the energetic neutral atoms and on the modeling parameters of the heliospheric plasma simulations.

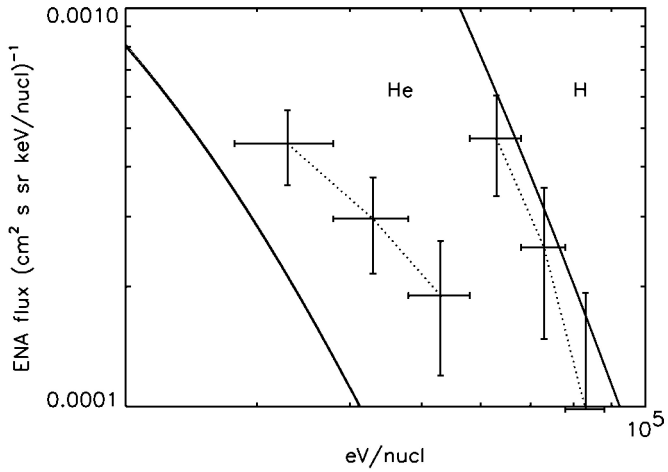

Figure 10. Best-fit H and He heliospheric ENA spectra compared with the HSTOF ENA data. The fits (thick lines) are using the lowest energy bins of the H and He spectra. The HSTOF data presented in the figure cover the forward part and flanks of the heliosheath (Czechowski et al. 2006). The heliotail sector is excluded. Vertical error bars show 1s statistical errors. Horizontal bars denote energy bins.

The low energy ion flux measurements by the LECP instrument on Voyager 1 downstream from the shock can be combined with the HSTOF ENA measurements to estimate the hydrogen column density in the heliosheath. With the ion spectrum given by the proton and helium in-situ post-shock data and the ENA spectrum by the CELIAS/HSTOF ENA data, the hydrogen column density can be determined. This approach presumes that the LECP ion fluxes can be used in place of the averages over the sector of the heliosheath covered by the HSTOF observations. The resulting hydrogen column density must be understood as an average over the same sector (within the apex or nose sector of the heliosphere, that is including both the forward part of the heliosheath and the flanks; Figure 10). The result of the simultaneous fit to the hydrogen and helium spectra corresponds to an average thickness within the selected sector of the heliosheath of about 75 AU (or about 30 AU in the apex direction). Based on this estimate from the CELIAS/HSTOF ENA and the LECP, Voyager 1 should leave the heliosheath region after the year 2024 (Czechowski *et al.* 2006, Hilchenbach *et al.* 2006).

...to the Interstellar Medium

The Solar Wind Meets the Interstellar Medium

Interstellar pickup ions. The *in situ* measurement of interstellar pickup ions with CELIAS CTOF makes it possible to observe part of the interaction of the interstellar medium with the solar wind.

These data yield valuable knowledge not only on the physics of interstellar neutral gas, but also on the plasma transport processes that occur in the solar wind after the ionization of the interstellar neutrals. Understanding these transport processes is critical to our knowledge of the near-Earth radiation environment.

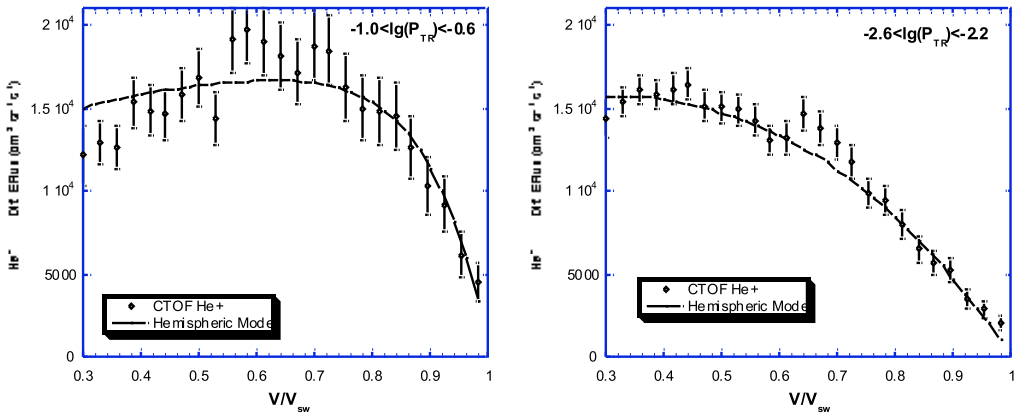

Figure 11. SOHO-CELIAS measurements of singly charged helium are shown for two different levels of transverse magnetic wave power P_{TR} in the solar wind as measured by the WIND spacecraft. Spectra are shown vs. the velocity of pickup helium, normalized to the solar wind velocity. The solid line represents the best fit hemispheric transport model for each case, where the fit is determined by varying the pitch angle diffusion rate (adapted from Saul et al., 2007).

The observed time variations and velocity spectrum of interstellar pickup ions are controlled by solar wind transport parameters including pitch angle diffusion rates, polytropic index (adiabatic cooling rate), compression/rarefaction rates, and other configuration and velocity space diffusion rates. The observation of pickup ion velocity distributions offers a rare opportunity to test plasma transport models. For example, Figure 11 shows the He^+ pickup ion distribution function obtained by CELIAS CTOF for two levels of transverse wave power in a near-radial interplanetary magnetic field, and the best fit using a hemispheric model of pitch angle diffusion.

Since the initial distributions of solar energetic particles accelerated in flares and coronal and interplanetary shocks are not well constrained, the observations of solar energetic particles do not validate transport models as well as pickup ion observations, where the initial distribution is well known. The measurements of interstellar pickup ions provided by CELIAS CTOF are a unique data set which makes it possible to probe quantitatively and in detail space-plasma transport processes.

Interplanetary hydrogen absolute ionization rates. Quémerais et al. (2006a) used SWAN measurements to derive the ionization rate of hydrogen and thus the solar wind mass flux during 1996-2005. The study covered variations of the anisotropy and absolute flux values, and clearly shows how the anisotropy of the hydrogen ionization rate evolves during the solar activity cycle from a

strong anisotropy at solar minimum to an almost isotropic ionization rate at solar maximum. These ionization rates will be used to derive the solar wind mass flux.

Two interplanetary hydrogen populations. Quémerais *et al.* (2006b) derived interplanetary H I Lyman α line profiles from the SWAN H cell data measurements obtained between 1996 and 2002. The profiles make it possible to examine the variations of the line profiles with solar activity. The SWAN results were compared to an interplanetary background upwind spectrum obtained by STIS/HST in 2001 March. Quémerais *et al.* found that the line-of-sight (LOS) upwind velocity associated with the mean line shift of the interplanetary Ly α line varies from 25.7 km/s to 21.4 km/s between solar minimum and solar maximum. Most of this change is due to variations in the radiation pressure. Line width (LOS temperature) measurements show that the interplanetary line is composed of two components scattered by distinct hydrogen populations with different bulk velocities and temperatures. This is a clear signature of the heliospheric interface in the line profiles observed at 1 AU from the Sun.

References

Aellig, M. R., Lazarus, A. J., & Steinberg, J. T. 2001, GRL, 28, 2767

Asbridge, J.R., Barrie, S.J., and Strong, I.B. 1968, JGR, 73, 5777

Asplund, M., Grevesse, N., Sauval, A.J., Allende Prieto, C., and Kiselman, D. 2004, A&A, 417, 751

Attrill, G., Nakwacki, M.S., Harra, L.K., Van Driel-Gesztelyi, L., Mandrini, C.H., Dasso, S., and Wang, J. 2006, Solar Phys., 238, 117

Bemporad, A., Raymond, J., Poletto, G. and Romoli, M. 2007, ApJ, 655, 576

Chandran, B. D. G. 2005, Phys. Rev. Lett., 95, 265004

Chen, J. et al. 1997, ApJ, 490, L191

Ciaravella, A., Raymond, J. C. and Kahler, S. W. 2006, ApJ, 652, 774

Cirtain, J. W., Del Zanna, G., DeLuca, E. E., Mason, H. E., Martens, P. C. H. & Schmelz, J. T. 2007, ApJ 655, 598

Cranmer, S. R., van Ballegooijen, A. A., and Edgar, R. J. 2007, ApJ Supp., 171, 520

Cranmer, S. R., Panasyuk, A. V., and Kohl, J. L. 2008, submitted to ApJ

Cremades, H. and Bothmer, V. 2004, A&A, 422, 307

Curdt. W., Wilhelm, K., Feng, L., and Kamio, S. 2008, A&A, *in press*

Czechowski, A., Hilchenbach, M., Hsieh, K. C., Kallenbach, R., Kóta, J. 2006, ApJ, 647, L69

De Pontieu, B. et al. 2007, Science, 318, 1574

Doschek, G.A. 2006, ApJ, 649, 515

Emilio, M., Bush, R.I., Kuhn, J., and Scherrer, P. 2007, ApJ, 660, L161

Fan, C.Y., Gloeckler, G., and Simpson, J.A. 1964, Phys. Rev. Lett., 13, 149

Fröhlich, C. 2006, Space Sci. Rev., 125, 53

García, R., Turck-Chièze, S., Jiménez-Reyes, J., Ballot, J., Pallé, P.L., Eff-Darwich, A., Mathur, S., and Provost, J. 2007, Science, 316, 1591

Georgoulis, M. and Rust, D. 2007, ApJ, 661, L109

Gömöry, P., Rybák, J., Kucera, A., Curdt, W. & Wöhl, H. 2006, A&A 448, 1169

Hansteen, V. 1993, ApJ, 402, 741

Heber, B., Posner, A., Rother, O., and Müller-Mellin, R., Implementation of Radiation Storm Forecasting with SOHO/COSTEP, European Space Weather Week, Brussels, 2007

Hilchenbach, M., Czechowski, A., Hsieh, K. C., Kallenbach, R. 2006, Observations of energetic neutral atoms and their implications on modeling the heliosheath, Physics of the Inner Heliosheath: Voyager Observations, Theory, and Future Prospects, 5th Annual IGPP International Astrophysics Conference, AIP Conference Proceedings, Vol. 858, p. 276

Hollweg, J. 2006, JGR, 111, A12106

Kahler, S.W. and Vourlidas, A. 2005, JGR, 110

Klassen, A., Gomez-Herrero, R., Boehm, E., Mueller-Mellin, R., Heber, B., Wimmer-Schweingruber, R.,

COSTEP/SOHO observations of energetic electrons far upstream of the Earth's bow shock, 2006, SOHO-17, (ESA SP-617)

Kocharov, L., Saloniemi, O., Torsti, J., Kovaltsov, G., and Riihonen, E., 2007a, ApJ, 654, 1121

Kocharov, L. et al., 2007b, ApJ, 659, 780

Kohl, J. L., Noci, G., Cranmer, S. R., and Raymond, J. C. 2006a, A&ARv, 13, 31

Krall, J. and St. Cyr, O.C. 2006, ApJ, 652, 1740

Kumar, A., and Rust, D. M. 1996, JGR, 101, 15667

Labrosse, N., Gouttebroze, P., and Vial, J.-C, 2007, A&A, 463, 1171

Lee, J.-Y. 2007, PhD Thesis, Kyung Hee University (South Korea)

Lee, J.-Y., Raymond, J. C., Ko, Y.-K. and Kim, K.-S. 2006, ApJ, 651, 566

Markovskii, S. A., Vasquez, B. J., Smith, C. W., and Hollweg, J. V. 2006, ApJ, 639, 1177

McIntosh, S.W. 2007, ApJ, 670, 1401

O'Shea, E., Banerjee, D. & Doyle, J. G. 2006, A&A 452, 1059

O'Shea, E., Banerjee, D. & Doyle, J. G. 2007, A&A 463, 713

Pagano, P. 2008, Ph.D. Thesis, University of Palermo (Italy)

Pagano, P., Raymond, J. C., and Reale, F. 2007, Bull. AAS, meeting 210, 29.111

Posner, A., 2007, Space Weather, 5, S05001, doi: 10.1029/2006SW000268

Quémerais, E., Lallement, R., Ferron, S., Koutroumpa, D., Bertaux, J.-L., Kyrölä, Schmidt, W., 2006a, JGR, 111, A09114

Quémerais, E., Lallement, R., Bertaux, J.-L., Koutroumpa, D., Clarke, J., Kyrölä, E., and Schmidt, W. 2006b, A&A, 455, 1135

Raouafi, N.-E., Harvey, J.W., and Solanki, S.K. 2007, ApJ, 658, 543

Saul L., Möbius E., Isenberg P., and Bochsler P. 2007, ApJ, 655, 672

Schmelz, J. T. & Martens, P. C. H. 2006, ApJ 636, L49

Schrijver, C. 2007, ApJ, 655, L117

Solanki, S.K., Krivova, N.A., and Wenzler, T. 2005, Adv. Space Res., 35, 376

Sterling, A. C., Harra, L. K. and Moore, R. L. 2007, ApJ 669, 1359

Švanda, M. Kosovichev, A.G., and Zhao, J. 2007, ApJ, 670, L69

Thernisien, A.F.R., Howard, R.A., and Vourlidas, A. 2006, ApJ, 652, 763

Tobiska, W.K., Bouwer, S.D., and Bowman, B.R, 2008, J. Atmos. and Solar-Terr. Phys., in press

Torsti, J., Riihonen, E., and Kocharov, L., 2004, ApJ, 600, L83

Wang, Y.-M., Sheeley, N.R., and Rich, N.B. 2007, ApJ, 657, 1340

Wenzler, T., Solanki, S.K., Krivova, N.A., and Fröhlich, C. 2006, A&A, 460, 583

Wills-Davey, M.J., DeForest, C.E., Stenflo, J.O. 2007, ApJ, 664, 556

Young, P.R. 2005, A&A, 444, L45

IV. The SOHO Bogart Mission

SOHO is unusual in the amount of realtime contact it currently enjoys: in order to downlink the scientific telemetry from the onboard recorder and allow the Flight Operations Team (FOT) to uplink commands for the roll steering law (RSL), spacecraft clock adjustment, and command loads for instruments not operated at the Experimenters' Operations Facility (EOF), *SOHO* typically receives 6.5 hours per day of Deep Space Network (DSN) coverage. In addition, roughly eight hours per day of additional DSN time allows the use of the MDI high-rate channels, which add 160 kbps to the ~ 44 kbps (including housekeeping telemetry) that normally goes to the recorder. For a single, 60 - 90 day continuous helioseismology campaign each year, *SOHO* receives nearly continuous DSN contact and thus continuous MDI high-rate telemetry.

DSN's ability to provide such generous support to *SOHO* has been predicated on the operation of single, 26-meter antennas at Madrid and Canberra (DSS-46 and -66), and of a 34-m antenna with similar characteristics at Goldstone (DSS-27), which are dedicated to serving Heliophysics missions. The 26-m antennas were built during the *Apollo* era in the 1960's and it is no longer practical to extend their service lives, so DSN will be shutting them down in 2008 and 2009 – if they last that long. That will allow two last continuous campaigns, in 2008 and 2009, the latter dedicated to intercalibrating MDI and the HMI instrument on SDO (see section V.c).

After the completion of MDI-HMI intercalibration, *SOHO* will complete its transition to the Bogart mission. MDI will be turned off, and EIT will be used for no more than a few, synoptic images per day (for comparing long-term response changes with that of the AIA telescopes on SDO). NASA will have no further requirement for observations from CDS, SUMER, and UVCS, so they are not included in the baseline budget. It should be noted, however, that ESA's extension of support for *SOHO* through the end of 2009 did not explicitly envision the retirement of any instruments. The "optimal" budget section of this proposal (Section V.G, below), presents scientific arguments for continuing observations by these instruments, as well as the required funding beyond the baseline.

Thanks to an "intermittent" recording scheme perfected by *SOHO* engineers for use during the worst parts of current telemetry "keyholes" (caused by the failure of the high gain antenna east-west drive mechanism in 2003) to preserve the helioseismology, TSI, solar wind, and when possible, coronagraph image data streams, it will be possible to reduce the effective *SOHO* telemetry bandwidth by more than a factor of three while allowing LASCO observing cadence and resolution to remain unchanged. A number of low telemetry rate but scientifically important measurements will be preserved at the cost of less than 25% additional bandwidth: GOLF (low l helioseismology and g-modes), VIRGO (TSI), SWAN (interplanetary hydrogen and solar wind anomalies), CELIAS (solar wind composition and plasma properties, absent magnetic field information; integrated solar EUV flux), COSTEP and ERNE (energetic, charged particles, including SEP early warning).

The lower telemetry rate achieved by turning off several *SOHO* instruments (Table IV-1) and the reduced daily spacecraft commanding requirements (see Section V.A) of the Bogart mission significantly reduce our realtime contact requirements. Since none of the instruments currently operated at the EOF other than LASCO will be operational in the baseline Bogart mission, requirements for near-realtime instrument commanding will be even more dramatically reduced. Even with a contingency of 1.0 - 1.5 hours per day in which to resolve communications anomalies, which are fre-

quent with the DSN, we estimate that no more than 4 hours a day of realtime contact will be necessary to operate the Bogart mission safely and with no loss of data.

***SOHO* Instrument**	**Bandwidth *SOHO* mission (kbps)**	**Bandwidth Bogart mission (kbps)**
GOLF	0.16	0.16
VIRGO	0.1	0.1
MDI	5.0 ; 160 (realtime only)	Off
SUMER	10.5 (submode 5) 0 (submode 6)	Off in baseline
CDS	12	Off in baseline
UVCS	5	Off in baseline
LASCO and EIT	7.8 (submode 5) 13.6 (submode 6)	LASCO only 13.6
SWAN	0.2	0.2
CELIAS	1.5	1.5
COSTEP	0.3	0.3
ERNE	0.7	0.7
Total	≤ 43.26 (all times) 160 (realtime only)	16.56
Daily DSN contact time needed (playback and spacecraft commanding only)	6.5 hr	2.5 hr
Daily DSN contact time needed for NRT instrument commanding)	3 - 8 hr	0.5 hr

Table IV-1. SOHO scientific telemetry requirements in the current mission configuration and during the Bogart mission.

V. Technical and Budget, FY08 - FY12

V.A The automation of SOHO operations

Starting in late 2006, in response to the budget guidelines from the previous Senior Review, the *SOHO FOT* began an in-house reengineering effort to automate *SOHO* mission operations. In the first phase of the transition from well-manned coverage of all contacts to complete automation with Observatory Engineers (OE's) on call, in 2007 September the FOT began the routine automation of all GSFC-local nighttime contacts. That followed three months of engineering trials when almost all night contacts were automated. The success of that effort gives us confidence that we can proceed to automate all contacts by the end of FY2008. Anomaly resolution and a restricted subset of critical spacecraft operations will continue to be carried out by the FOT; otherwise, they will construct a pass plan in advance that contains all command procedures and loads. The automation software directs the commands to the existing TPOCC software, and COTS anomaly detection and notification software notifies the OE's and appropriate experiment team members (in case of an instrument anomaly). One major simplification will result from discontinuing daily roll steering law updates to keep the *SOHO* spacecraft Z axis aligned with the solar rotation axis; instead, the spacecraft will be allowed to maintain its natural orientation with respect to the ecliptic. (Maintaining the spacecraft Z-axis with constant orientation with respect to the solar rotation axis was an MDI requirement; without that maintenance, LASCO images can be rectified on the ground.)

FOT compliment (FTE)	"Classic" SOHO	Current	Bogart mission
Observatory engineers	4.45	5.55	4.40
Console operators	9.90	4.40	None
DSN schedulers, others	7.70	5.36	1.19
Total	22.05	15.31	5.59

Table V-1. SOHO Flight Operations Team staffing before 2006 ("Classic"), after the first phase of operations automation ("Current"), and during the Bogart mission.

As shown in Table V-1, the size and skill mix of the FOT will change as well: we expect to eliminate the console operator positions by the beginning of the Bogart mission, since all of their non-commanding functions will have been replaced by the automation software. The automation reengineering effort will nominally be carried out using only FOT labor.

In parallel with the automation effort, a reengineering of the EOF Core System (ECS) is planned for FY08 to guarantee reliability and robustness throughout the Bogart mission, currently budgeted at $50K but with 100% contingency, since such efforts are often extended when unexpected configuration issues are discovered.

V.B Risk mitigation in a fully automated scenario

We would be remiss if we did not discuss the risks assumed by the transition to automation. Foremost among these are the possibility of inadequate notice of a critical anomaly, and failure to be able to act in time to correct a mission-threatening situation in a timely fashion. The COTS monitoring and notification software provides for full and timely FOT insight into the nature and seriousness of the anomaly. Timeliness of notification is clearly important, but twelve years of *SOHO* operations have shown that we never want to respond too quickly to a spacecraft anomaly; indeed, experience has shown that a series of meetings of program management, operations teams, and engineers beginning the next working day is always adequate to insure both the efficient use of onboard resources and fastest *safe* recovery of science operations. The Emergency Sun Reacquisition (ESR) mode into which the spacecraft falls in the case of serious anomalies is stable for up to 48 hours, and ground intervention at scheduled contacts (more frequent in the case of spacecraft anomalies) minimizes thruster fuel usage. With fewer instruments operational, full recovery will probably be faster than currently, even with less DSN contact. We are also able to call upon the experience of numerous missions operated by GSFC, including the ACE mission at L1, to conclude that anomaly rates actually decrease when operations are automated. Most importantly, the reduction in size of the FOT is counterbalanced by the expertise of the staff, which will consist primarily of veteran Observatory Engineers who are intimately familiar with the spacecraft and ground system.

V.C MDI-HMI intercalibration

While SDO HMI will be taking all possible observations, all the time, MDI is limited to “low rate” (5 kbps) observations when *SOHO* is out of realtime contact. Higher-bandwidth (160 kbps) meaurements, including observations in MDI’s high-resolution subfield, are possible only during periods of realtime contact. Intercalibration of MDI and HMI will therefore require extended realtime “continuous campaigns” as well as uninterrupted time series of low-rate data.

Considerable work has gone into comparing MDI and groundbased network (GONG) data, since differences between the two appear attributable in all cases to systematic errors unique to one data source or the other, caused by imperfections in both instruments (GONG is considered here as a single, complex "instrument"). Intercalibration of MDI and SDO HMI should be easier, since atmospheric “seeing” will not be present. The Stanford team (PI for both MDI and HMI) is confident that they will be able to intercalibrate sufficiently that they can create a seamless dataset across the mission boundary, *as long as there is sufficient overlap*. The expected period of systematic variations for HMI is one day, with the 3.2 km/s geosynchronous orbital velocity leaking into the Doppler signal. For MDI, the equivalent period is one year, for the 0.5 km/s orbital LOS Doppler signal amplitude. MDI is retuned twice a year to minimize the net offset velocity with respect to the wavelength sampling positions. In a span of 135 days, MDI and HMI will sweep the full range of velocity zero offsets of both instruments. This is roughly ***two 72-day basic time series segments***; 72-day sequences of low-rate data are the basis of many MDI helioseismology studies including interior rotation. An intercalibration of that duration will allow sampling of the full range of MDI calibration uncertainties and be able to generate a compatible HMI time series that will enable tracking of the internal solar rotation in a continuous series spanning both missions.

The MDI continuous contact campaigns provide the prime data used for "local helioseismology" studies of the whole Sun for studies such as meridional circulation which is important for understanding the 11-year cycle. Having at least one 60-day campaign, which gives two solar rotations, will allow cross calibration of the two instruments for full-Sun, nonrotational flows. One of the big improvements expected with SDO HMI is continuous coverage of the whole solar disk. Intercalibration with the 12-year record from MDI will allow studies of such topics as meridional flow to be extended to the full baseline of the two missions. Just as with the medium-*l* data obtained during SOHO low-rate times, the high-rate, full resolution, full disk data obtained in the continuous contact intervals has systematic errors which introduce artifacts into the inferred solar flows. These are again variations across the field of MTF and distortions at the sub-pixel level. The HMI distortions are less, but not zero, and certainly different. Since the distortions are large in scale they couple into large scale inferences of solar flows. ***Two solar rotations***' overlap of full disk coverage should be considered the minimum to allow sufficient characterization of the differences between the two instruments.

In addition to different orbits and different filter and image quality variations across the field, MDI and HMI will observe the Sun in different spectral lines. Based on an extensive study that led to the selection of the HMI line, both lines are believed to sample the same part of the photosphere, but the HMI line is more sensitive to magnetic fields. The leakage of magnetic field induced variations in the line profile into the Doppler signal will certainly be different for the two instruments. Likewise, differences in the measured Doppler signals are expected because of the sampling method (MDI, one polarization; HMI, two). Thus, the linearity and cross field variations in both Doppler and magnetic signals will be different between the two instruments. A intercalibration while observing the same Sun is important. The total coobserving time (two 72-day periods of MDI low-rate data plus a 60-day continuous contact campaign) required for both the characterization of MDI and HMI image distortions and the removal of orbital velocity effects should be adequate to characterize the different responses of the two spectral lines to a variety of solar features.

The transition from the nominal *SOHO* mission to the Bogart mission will therefore depend on the realization of the MDI-HMI intercalibration requirements. As soon as they have been met, MDI can be powered down and *SOHO* operations scaled back to the Bogart levels.

V.D SOHO to Bogart transition

FY09 will be a year of transition from the *SOHO* mission to the Bogart mission. Under the baseline plan, UVCS, CDS, and SUMER will be turned off, and MDI will complete its intercalibration with HMI before being turned off as well. (Note: a significant slip in SDO launch date could cause the actual end of the intercalibration to slip into FY10.) After a shorter period of intercalibration with SDO Advanced Imaging Array (AIA), EIT will also stop observing, except for infrequent, four-wavelength “synoptic sets” to monitor long-term throughput changes.

At the beginning of FY10, the LASCO workstations and the EOF Core System (ECS) will be moved to Building 21 at GSFC, which houses the Heliophysics Division, and the *SOHO* EOF will be abandoned. The Mission Operations Center (MOC) and a facility for the non-resident PI teams' workstations will remain in their current location in Bldg. 3.

V.E SOHO to Bogart: science team funding

With the exception of the CELIAS instrument (a foreign PI-led effort with a lead US Co-I), funding for US science teams will be phased out in FY09. Thereafter, LASCO will be operated by 1.5 FTE of skilled operators of the instrument who have worked under contract directly to NASA for several years, and will continue to do so in the Bogart mission. The operators will also be responsible for the maintenance and administration of the ECS, which enables near-realtime commanding between science teams' workstations on the Open IONet and the *SOHO* Command Management System (CMS) on the more secure Restricted IONet. As part of the planning for the Bogart mission, we examined whether the ECS and CMS were necessary, and concluded that they were: the FOT uses the CMS to build command loads, and we need a secure gateway between the investigators' workstations and the CMS. (Under nominal operations, only LASCO will be using the ECS interface, but each of the other operational instruments maintains a workstation at the EOF for anomaly resolution.) The LASCO PI team engineering expertise will continue to be available, on call, if instrument anomalies occur.

The UVCS and LASCO teams will be funded in FY2009 for the final archiving of their mission data and their submission to the mission archive (See MAP). MDI will be funded in FY09 for the intercalibration effort (see Section V.C), a final analysis of a solar activity cycle's worth of helioseismology measurements that will also serve to validate the data for archiving in FY2009, and the final archiving itself in FY2010.

V.F Budget

FY09 will see the dramatic change in scope between the nominal and Bogart missions: US PI and lead CO-I teams (except for CELIAS) will be phased out, the FOT will be reduced to a level appropriate for operating a SMEX-class mission without sacrificing expertise, and mission archiving will be completed. FY10 and after are foreseen to be a steady state, so long as *SOHO* is able to contribute to SDO and the larger Heliophysics Great Observatory effort.

In FY08, we will complete the automation of all *SOHO* ground station contacts other than maneuvers and anomaly resolution. Similarly, we will upgrade and rightsize the EOF Core System (ECS), which is currently hosted on a 15-year-old, obsolete platform by porting it to Linux; ECS reengineering is likely to involve 0.25 - 0.50 FTE of effort this year, with a smaller commitment in FY09 to insure a smooth transition.

The budget figures in Table V-2 are organized differently from the ones in the Senior Review standard format (separate spreadsheet and Table V-3); they are organized by actual commitments that the US Project Scientist has to meet in order to insure the scientific success of the mission.

In both FY08 and FY09, there are contingencies to cover FOT overtime in case automated operations do not provide adequate response to ground station configuration issues during MDI continuous contact campaigns, including the crucial MDI-HMI intercalibration periods in FY09. The larger contingency figure in FY08 also covers any labor from outside the FOT that may be necessary to complete automation of operations in a timely fashion.

*Table V-2. The SOHO and Bogart budget as the project scientist sees it every day. All figures in $K. Note that the totals for FY11 and FY 12 are **below** the baseline guideline.*

Each of the US PI or lead Co-I teams is funded at a low level in the year after their operations cease, to complete and submit their mission archive. (See Mission Archive Plan; separate document.) UVCS and CDS science operations end in mid-FY09 (assuming an SDO launch by early calendar year 2009), and EIT operations end even earlier, after one solar rotation of co-observing with SDO

*Table V-3. The baseline SOHO and Bogart budget as required for this proposal. All figures in $K. Totals for FY11 and FY12 are **below** the baseline guideline.*

AIA – thus the substantial drop in LASCO EIT costs at Goddard from FY08 to FY09. The LASCO figures in the FY11 and FY12 columns represent contingency to cover support from the original PI institution's engineering staff in case of instrument anomaly. If unused, it will be returned to the MO&DA program. The bump in "other mission expenses" in FY11 represents the replacement of the hardware holding the *SOHO* archive.

Civil service labor at Goddard in the Bogart mission is reduced to a US Project Scientist/LASCO operations/EIT archiving scientist (0.6 FTE), a resource analyst (0.5 FTE), and 0.25 FTE of a Mission Operations Director's time. As long as *SOHO* is operated as an independent mission, that appears to be the lowest level of support institutionally possible.

The "full-cost communications" line is a new one, instituted by the NASA Integrated Services Network (NISN) to show full-cost accounting for the use of IONet tail circuits, Voice and Data System (VDS) boxes used in mission operations, and related costs. We are reducing the number of VDS boxes used by *SOHO*, and will monitor efforts by SSMO to control these costs.

The *SOHO* mission operations director, FOT, and FOT contractor deserve full credit not only for their work on the automation of *SOHO* operations, but also for working to reduce FOT staffing dramatically while retaining crucial expertise and minimizing operational risk. As a result, we believe that after the mission archiving effort in FY10, we should be able to operate the *baseline* Bogart mission significantly below the budget guidelines for FY11 and FY12.

V.G "Optimal" scenarios

V.G.1 Science cases

UVCS. UVCS is the only instrument that could be operating in 2009 - 20012 that can measure key plasma properties in the acceleration of the solar wind and in CMEs. Those measurements are essential to testing models of coronal heating, solar wind acceleration, SEP production in CMEs, and CME evolution – and are thus central to Heliophysics scientific objectives. Combined observations from UVCS and LASCO on *SOHO*, RHESSI, *Hinode*, STEREO, and SDO should give a much more complete picture of plasma heating, ion acceleration, and CME shocks than was possible in the same phase of the previous solar cycle.

CDS. While the EIS spectrometer on *Hinode* supersedes CDS to some degree, the CDS NIS can access lines from several more species (including ions of Fe, Si, Al, Mg, Ca, Ne, N, O, and He), and EIS is largely limited to sampling plasma at coronal temperatures; bright, unblended lines at cooler, transition region temperatures are unique to CDS. Unlike EIS, CDS can produce high-cadence time series with excellent pointing stability over long time intervals, and its selection of targets on the disk and low corona is fully flexible, unrestricted by the spacecraft pointing and independent of activities of other *SOHO* instruments – EIS must observe wherever *Hinode* is pointed.

Only CDS and SUMER can currently provide measurements of Doppler velocities of the cool ($log\ T_e \sim 5.5$ - 6.0) filament material associated with nearly all leading to CMEs, in CDS's case, through access to lines of He I and O V (Sterling, Harra and Moore, 2007). CDS will thus be the only available source of spectroscopic characterization of the underlying, cool plasma involved in eruptive events observed with SDO AIA during the rise of the new solar cycle. The latest modeling of He I 584 and 537 Å resonance lines (Labrosse et al. 2007) shows that the He I line profiles are sensitive to Doppler dimming effects and provide excellent diagnostics of thermodynamic parameters of erupting prominences.

SUMER. SUMER is and will continue to be the only high resolution spectrometer able to observe spectral lines formed across the temperature range from 4200 K (molecular hydrogen) to 10 MK (Fe XXI), and, in particular, to capture the dynamics of the transition region/low corona (0.1 to 0.6 MK) down to 2 km/s in a large variety of lines from different ions (C III, Si IV, NV, O V, O VI, Ne VIII). Only SUMER can provide detailed spectroscopic information on the structure of the chromospheric and TR network for comparison at a spatial resolution (1") comparable with that of SDO AIA EUV images and SDO-HMI magnetograms. The *Hinode* EIS (EUV) spectrometer has proved invaluable for measuring flows in the hot (1 MK) plasma but the footpoint emission (0.1 MK) is much stronger in the longer-wavelength UV and SUMER exposure times are almost a factor 10 shorter than EIS for observations of this cooler plasma. SUMER is also the best instrument for monitoring filament activity and, due to its unique access to the H I Lyman series, to diagnosing filament properties prior to eruption.
SUMER off-limb observations have revealed Doppler shift oscillations in coronal loops, high Doppler shifts (1000 km/s) in downflows and at flare onset indicative of magnetic reconnection. Today, STEREO EUVI and *Hinode* XRT images of coronal plasma provide the context for events observed by SUMER with unprecedented information content; after 2009, LOS Doppler information from SUMER will complement the high-resolution and high-cadence SDO AIA images.

V.G.2 Instrument lifetime considerations

UVCS. UVCS continues to be capable of performing all of its primary science observations. Star observations reveal that UVCS radiometric responsivity has decreased by 11% per year since 1998, at 2 solar radii, with lower rates of decrease at larger heights. All UVCS mechanisms are nominal except the sluggish Lyα grating drive. The Lyα detector retains its original sensitivity over the entire detector area, and the OVI over 60% of its area. Both detectors have a problem that shifts the counts in some 64 row groups to the first row of the group. The spectra, however, are not affected, as the count shifts are only in the spatial dimension. After full binning, 10 arc min of the spatial areas retain their original spatial resolution and 30 arc min have a spatial bin size of 7.3 arc min,

appropriate for coronal holes. Currently, about 24 arc min (60%) of the detector areas retain their full spatial resolution.

CDS. CDS is in good health and carries no consumables. All subsystems are nominal, and continued updating of the NIS wavelength calibration accounts for the effects of the secular warming trend on the front of the spacecraft. The sensitivity of the NIS microchannel plate (MCP) continues to degrade slowly, but is expected to produce less than a factor of two additional degradation over the next six years. The PI team continues to monitor the sensitivity decrease and apply corrections in standard data analysis software.

SUMER. There will be no limitations in using the azimuth drive for rastering. Because the SUMER XDL detectors are at or very near their maximum gain limits, some limitations will apply for high photon input over longer periods of time.

V.G.3 Technical and management considerations

The extension of the *SOHO* mission to provide LASCO imagery to meet SDO scientific objectives was first discussed with Heliophysics management in 2003 October, and did not envision the continuation of CDS, SUMER, or UVCS science operations. CDS's capabilities have been partially superseded by the EIS instrument on *Hinode*, and until recently, the SUMER offset pointing capability was constrained to a single axis. All three instruments, but particularly CDS and SUMER, require substantial additions to the number of hours of daily DSN contact for telemetry downlink (see Table V-4).

To accommodate telemetry "keyhole" periods, an "intermittent recording" scheme was developed to optimize the use of the onboard recorders. None of these scenarios, however, involves SUMER, so additional development would be needed to operate SUMER during the Bogart mission while retaining the current LASCO bandwidth. The development effort would have to be carried out by an ESA contractor responsible for the onboard Command and Data Handling subsystem. The telemetry bandwidth currently enjoyed by LASCO is at the expense of SUMER: SUMER must be off for LASCO to achieve its current image cadence, and operating SUMER drops the LASCO bandwidth by approximately half. It should be noted that for the last several years, the SUMER PI has only had the resources to operate the instrument for two campaigns of roughly two weeks duration (each) per year.

As can be seen from Table V-4, the downlink requirements grow rapidly with the addition of CDS (12 kbps) or SUMER (10.5 kbps), and only UVCS (5 kbps) represents a marginal addition.

Configuration	Downlink contact hours required per day
Baseline Bogart mission	2.5
Bogart + CDS only	3.8
Bogart + SUMER only *	3.5*
Bogart + UVCS only	3.1
Bogart, CDS, SUMER *	4.2*
Bogart, CDS, UVCS	4.5
Bogart, SUMER *, UVCS	5.0*
Bogart, CDS, SUMER, UVCS	6.0

Table V-4. Approximate downlink requirements for various optimum scenarios. All figures include margins for pass setup and spacecraft acquisition. The starred cases would either decrease the total LASCO bandwidth by more than 50%, or require currently unbudgeted modifications to the telemetry allocation scheme by an ESA contractor. SUMER, however, would only be operated in campaigns of two weeks' duration.

Except for the addition of additional DSN scheduling support (~ 0.25 FTE per year) to accommodate a larger downlink requirement, none of these mission operations scenarios should entail extra costs to the Bogart mission. The UVCS team has developed a simplified science operations scenario requiring only remote commanding; the budget for continuing UVCS operations is folded into the "optimum" budget matrix in Table ***V-5***.

It is important to note that the resulting, "optimum" budget exceeds the *baseline* budget guideline only in fiscal year 2010; in FY11 and FY12, it still falls *below* the baseline budget. The minimal amounts for scientific data analysis shown for FY10 and later provide just enough analysis to validate the scientific data products.

It is also worth noting that as CDS and SUMER are supported solely by European national funding agencies after FY08, there is no impact to the *SOHO* Bogart mission budget to extending their operations as long as funding and/or instrument operability persist. There *will* be a considerable impact on DSN scheduling, and it is not clear whether DSN can accommodate continued operations of all *SOHO* instruments but MDI. SUMER would only be operated in two or three campaigns per year, however, so the demand for DSN time is somewhat mitigated.

*Table V-5. The optimal SOHO and Bogart budget; all figures in $K. This is identical to Table V-3, other than the addition of (i) increased DSN scheduling labor (line 2.b) and (ii) a barebones budget for continuing remote operation of UVCS by the PI team (line 3). Note that this "optimal" scenario for the Bogart mission (years FY10 and later) comes in **below** the **baseline** budget in FY11 and FY12; only in FY10 would additional funds be necessary.*

*Figures in **red** represent increases over the **baseline** budget; figures in **blue** represent underguides.*

VI. Education and Public Outreach

Education

SOHO educational activities are generally carried out by the two US PI teams at major universities (MDI at Stanford and UVCS at the Harvard-Smithsonian Center for Astrophysics), and though drastically scaled back in the years covered by this proposal, those activities will continue at some level well below 1 - 2 % of the total *SOHO* or Bogart mission budget. Many of those activities are already carried out on a volunteer (no cost to NASA) basis. Given the extremely limited budget in the years FY09 and FY10, and the phasing out of both of the teams most responsible for educational activities in the baseline budget, however, we list no education component in our budget.

Outreach

Given the dramatic new imaging and video coming from *Hinode* and STEREO, it is only appropriate for *SOHO* to take a back seat in outreach, particularly as we prepare to be eclipsed by the awesome potential of SDO for communicating the drama of the solar atmosphere. We will continue to run *SOHO* "Hot Shot"stories when scientific news breaks, usually in conjunction with NASA and/or ESA press releases, and we will continue to fulfill every request from the media for *SOHO* material, but it is simply more appropriate for the newer solar and heliospheric missions to grab the spotlight that *SOHO* and TRACE nearly monopolized for twelve years. Since outreach activities will be driven primarily by other missions in the years covered by this proposal, therefore, we do include them in our baseline budget, but instead plan to deal with the very low level of costs likely to be incurred out of contingency in our "other expenses" budget line.

Appendix A. SOHO publication record, 2006 - 2007

SOHO refereed publication rates through the first few weeks of calendar year 2008 can be found in Table A-1.

Calendar Year	Refereed Journals only
1996	31
1997	125
1998	174
1999	297
2000	295
2001	210
2002	289
2003	305
2004	332
2005	330
2006	273
2007	351
2008 (through April 8)	76
Total	3088

Table A-1. SOHO refereed papers

Here, a "*SOHO* paper" is taken to mean any paper using *SOHO* data, or concerning models or theoretical interpretations of *SOHO* measurements.

"Market share" In the years since the launch of *SOHO*, there have been over 3,000 different authors and co-authors of *SOHO* papers in refereed journals. Since *SOHO* carries both *in situ* and remote sensing instruments, there is a large potential pool of authors. Considering just the remote sensing instruments, there are roughly 600 members of the AAS Solar Physics Division and a roughly equal number of active solar physicists in Europe and Asia (combined). Past experience indicates that approximately 75% of those are "active," in the sense of publishing at least one refe-

reed paper per year, so *SOHO* is clearly serving a large number of members of the heliospheric community as well.

Publication rate. Despite reduced funding for scientific analysis of *SOHO* data both in the US and the countries of the European Principal Investigators over the last two years, the *SOHO* publication rate has remained healthy; the dip in 2006 may be due to the large number of *unrefereed* papers contributed to the proceedings of the workshop held in Sicily to commemorate the tenth anniversary of the beginning of the scientific phase of the *SOHO* mission. The same cause may lie behind the record number of publications in 2007.

We are convinced that this success is based on the open and convenient accessibility of *SOHO* data and analysis software. Only a data policy of this type is likely to draw in the widest possible scientific community — including amateurs — to the enterprise of mining S3C data for their maximum scientific return.

Bibliography. A listing of *SOHO* publications in refereed journals for the years 2006 – 2008 can be found at http://umbra.nascom.nasa.gov/soho/sr08/soho_publ_2006_2008.html .

Appendix B. Instrument Status, 2008 January 28

GOLF

- Operating nominally, with data continuity ~98% outside *SOHO* 1998-1999 "vacation" periods, including no losses during telemetry "keyholes"
- Overall throughput down by a factor of <7 since launch, but:
  - largest noise source is the Sun itself, so negligible adverse effect over most of the frequency range, including that in which the *g*-modes are expected
  - significant reduction in signal to total noise ratio in a region around 1 mHz
- No reason to doubt that GOLF can continue to function in its present mode for several years
  - Complete redundant channel still available, though unused since initial, on-orbit commissioning

VIRGO

- All VIRGO instruments (the two types of radiometers: PMO6V and DIARAD, the filter radiometers SPM, and the luminosity oscillation imager LOI), are fully operational and performing properly. The degradation of sensitivity is still relatively small and all the instruments are still able to achieve the same accuracy and precision as at launch.

MDI

- ~90,000,000 images; after on-board computations, ~15,000,000 raw data images downlinked
- Expected degradation in total light throughput due to changes in the front window; compensated *via* increased exposure time.
  - mean annual degradation: 4%, appears constant
- Electronics anomaly in 2007 was corrected by instrument power cycle
- Exposure time uniformity: sudden drop in 2000 March, from a part in 12000 to a part in 4000
  - affects helioseismology only for $l < 4$
  - adds some noise to zero point of photospheric magnetic field measurements; correctable
  - No variations above the one part in 4000 level since 2002 February reduction in optics package temperature
  - No detected change in the CCD flat field except for variations with focus change
- The drift in central wavelength of the Michelson's has nearly stopped
- The drift in best focus position has moved the nominal focus setting back almost to the design point. Shortly after launch it was at the limit of the adjustment range.
  - This drift has also apparently slowed
- In summary, no known limit to MDI's useful life

SUMER

- Pointing mechanism has worked flawlessly during the recent years and restrictions on pointing will be released, since detector lifetime is regarded as the most critical resource
- Detector A can only be operated with reduced spatial resolution (MCP anode electronics degradation); an investigation of the problem in the address decoding electronics has shown that the effect is tempera-

ture dependent. Mitigation by operating at higher temperatures is, however, only partial and not a permanent solution. Consequently, the A-detector is no longer used.
- Detector B fully operational and will remain radiometrically calibrated for another 2-3 years, based on extrapolation from past performance

CDS

- GIS nominal; no recalibration or changes to high voltages have been necessary in the past 3 years.
- NIS nominal; microchannel plate current anomaly in 2005 July appears to have been self-healed after a series of tests and is being used for regular observations again; sensitivity in short wavelength channel 40 - 80% of pre-launch levels; expect drop to no worse than 20 - 60% if CDS is operated throughout the Bogart mission
- Electronics nominal; trending shows no aging of components
- Mechanisms: Some 'stickyness' when rastering the GIS slits necessitated a small restriction on the range of movements. This has now been compensated for by improved ground planning software that moves the allowed range of movements to outside of the restricted area. This issue no longer impacts on science. All other mechanisms continue to operate nominally.
- Thermal: As with all other components of *SOHO*, the sunward side of CDS shows a secular increase in temperature, but analysis of the science data shows that the NIS wavelength calibration remains within tolerances.
- Onboard software: No issues

EIT

- EIT is nominal
- Instrument throughput decrease stopped and reversed since 2003 (see: http://umbra.nascom.nasa.gov/eit/eit_guide/euv_degradation.html)
    - Reversal due to long bakeouts occasioned by telemetry keyholes
    - CCE loss can be tracked accurately with calibration lamp images
    - Degradation now understood and modeled
    - Present exposure times range from 12 s (195 Å) to 2 m (284 Å): lots of latitude left
    - Current throughput at 195 Å is comparable to that in mid-1999

UVCS

- Both UVCS detectors are affected by an analog-to-digital converter (ADC) issue that shifts counts in some groups of 64 rows into the first row of the group. SUMER, which has similar detectors, has seen a more rapid degradation, in which it appears that the worst possible state would leave all but the first 97 rows of each detector affected, and thus degrade the effective angular resolution of the instrument to 7 arc min. Even if that were to occur, the spectral lines could be positioned on the unaffected rows.
- Radiometry: The degradation of the responsivities varies with the largest deterioration at the lowest observed heights. For 2.0 R_{sun} ,the OVI channel responsivity is degrading at 15% per year. In 2009, it will be 16% of the original value, and in 2012, it will be 11%. The Lyα rate is 12% per year and so it will reach 25% of the original in 2009 and 19% in 2012. In any case we will continue to monitor this using star observations and coronal vignetting scans.

- Visible light detector: Experienced an anomaly in its housekeeping telemetry system and was turned off in 2004 April. Since its principal function of verifying the LASCO electron density measurements and co-registration has been accomplished, the risk of further operation is not justified.
- Mechanisms: All mechanisms continue to behave nominally except for the Ly a grating drive, which is slow to respond when commanded; has not prevented this channel from being used for high priority science.

LASCO

- Thernisien *et al.* (2005) have performed a detailed analysis of the intensity of a set of about 50 moderately bright stars that transited through the C3 field of view
    - These 50 stars generated about 5000 observations during the lower cadence in the first three years of *SOHO* operations and about 15000 observations thereafter
    - All stars have spectra well known from 13-color photometry
    - Using these stellar spectra as standards and the observed LASCO count rates, derived the photometric calibration factors of the C3 coronagraph for all five color filters with an absolute precision of ~7%
    - Decrease in the instrument sensitivity found to be only ~3.5% over the 8 years studied or < 0.5% per year
- C2 response changes similar; still under investigation
    - Final calibration expected before end of 2005
- The Fabry Pérot interferometer in the C1 coronagraph did not survive the extreme cold the instrument experienced (-80C) during the 1998 *SOHO* offpointing

CELIAS

- MTOF/PM, STOF/HSTOF, SEM nominal
    - MTOF, PM efficiency degradation of 2 (Fe) to 5 (H); still extremely high S/N
    - STOF performance stable, MC degradation compensated for by increase in HV
- CTOF impaired since 1996 October (HV power supply hardware failure)

COSTEP

COSTEP consists of two sensors, the Low-Energy Ion and Electron Instrument (LION), and the Electron, Proton, and Helium Instrument (EPHIN). Both instruments have suffered some degradation but continue to generate valuable scientific data and fulfill their scientific goals.

- LION: Unexpectedly high noise level in the LION detectors since shortly after launch have resulted in the loss of the lowest energy channels (< 80 keV). In the course of the mission, three of the four LION sensor heads developed disturbances, some of which can be mitigated by careful data analysis. The disturbed periods are well documented in the level-2 data specification document. As of January 2008 one sensor head is still functioning nominally.

- EPHIN: Detector E of the EPHIN instrument showed steadily increasing noise levels throughout 1996, and had to be switched off (on October 31, 1996) to guarantee reliable measurements with the instrument. By changing the instrument configuration, the EPHIN measurements can still be achieved with

slightly degraded energy resolution in a limited energy range (3-10 MeV for electrons and 25-41 MeV/n for ions). This detector behavior causes no significant degradation of the scientific goals of EPHIN.

ERNE

- Secular increase in temperatures at front of spacecraft has caused increased detector leakage currents. Including radiation effects, the increase during the last five years has been roughly 20 $\%yr^{-1}$.

- One of the detector channels of the topmost ERNE/HED detector layer malfunctioned on 2000 November 21. Updated onboard software accounts for this issue: the geometrical acceptance (view cone) of the detector is unaffected, as is the measurement of the heavy nuclei (Carbon and heavier). Also the light nuclei are unaffected up to an energy of ~ 20 MeV/n. Between 20 MeV/n and 120 MeV/n (maximum energy measured by ERNE), both the coordinate and energy values of the affected detector become increasingly unreliable. This, however, has no effect on particle identification and produces only marginal statistical fluctuation on the total energy of these particles that deposit most of their energies in the lower detector layers.

SWAN

- Instrument status unchanged since 2001
    - All four motors nominal
    - +Z hydrogen absorption cell nominal; -Z cell empty: no absorption when activated (loss occurred in 2001)
    - Both sensors calibrated using HST STIS reference spectra: +Z sensor response constant since 1998 (outside of adjustments for high voltage [HV] setting), -Z sensor response shows decline of ~ 10% per year. HV setting changed to compensate as much as possible

Appendix C. Acronyms

ACE	Advanced Composition Explorer
AIA	Advanced Imaging Array (SDO)
CDS	Coronal Diagnostic Spectrometer
CELIAS	Charge, Element, and Isotope Analysis System
CIR	Corotating interaction region
CISM	Center for Integrated Space Weather Modeling (NSF supported)
CME	Coronal mass ejection
CMS	Command Management System
COSTEP	Comprehensive Suprathermal and Energetic Particle Analyzer
COTS	Commercial, off the shelf
CTOF	Charge Time-Of-Flight sensor of CELIAS
DIARAD	DIfferential Absolute RADiometer (active cavity radiometer) component of VIRGO
DSN	Deep Space Network
EAF	Experimenters' Analysis Facility
ECS	EOF Core System
EIT	Extreme ultraviolet Imaging Telescope
ENA	Energetic neutral atom
EPHIN	Electron, Proton, and Helium INstrument (part of COSTEP)
ERNE	Energetic and Relativistic Nuclei and Electron experiment
EOF	Experimenters' Operations Facility
ESA	European Space Agency
EUV	Extreme ultraviolet
EVE	Extreme ultraviolet Variability Experiment (SDO)
FDF	Flight Dynamics Facility
FOT	Flight Operations Team
FTE	Full time equivalent (one person's work in one year)
FY	Fiscal year
GIS	Grazing Incidence Spectrograph of CDS
GOLF	Global Oscillations at Low Frequencies
GONG	Global Oscillation Network Group
HGO	Heliophysics "Great Observatory"
HMI	Helioseismic and Magnetic Imager (SDO)
HST	Hubble Space Telescope
ICME	Interplanetary coronal mass ejection
IONet	Internet Operational Network (NASA)
IP	Interplanetary
L1	First Lagrangian libration point
LASCO	Large-Angle and Spectrometric Coronagraph
LOI	Luminosity Oscillations Imager component of VIRGO
MDI	Michelson Doppler Imager
MO&DA	Mission Operations and Data Analysis
MTF	Modulation transfer function
MTOF	Mass Time-of-Flight mass spectrometer of CELIAS
NIS	Normal Incidence Spectrograph of CDS
NSSDC	National Space Science Data Center
OMNI2	NSSDC composite data source for heliospheric measurements [*]
OE	Observatory Engineer

PFSS	Potential-field source surface
PM	Proton Monitor of CELIAS MTOF
PM06	Twin-cavity radiometer component of VIRGO
SAO	Smithsonian Astrophysical Observatory
SDO	Solar Dynamics Observatory
SEM	Solar EUV monitor of CELIAS
SEP	Solar Energetic Particle
SOHO	Solar and Heliospheric Observatory
SOI	Solar Oscillations Investigation
SMEX	Small Explorer
SPM	Spectral irradiance monitor component of VIRGO
STEREO	Solar TErrestrial RElations Observatory
STIS	Space Telescope Imaging Spectrograph
STOF	Suprathermal Time-of-Flight ion telescope, part of CELIAS
SUMER	Solar Ultraviolet Measurements of Emitted Radiation (UV spectrometer)
TRACE	TRansition Region And Coronal Explorer
SWAN	Solar Wind Anisotropies
UVCS	Ultraviolet Coronagraph Spectrometer
VIRGO	Variability of Solar Irradiance and Gravity Oscillations
VSO	Virtual Solar Observatory
XDL	Cross Delay Line

SOHO instrument names are in blue.

[*] The OMNI2 data cited in this proposal were obtained from the Magnetospheric State Query System developed and created by the Space Physics Data Facility of NASA Goddard Space Flight Center.